

Quenching Dynamics of a quantum XY spin-1/2 chain in presence of a transverse field

Victor Mukherjee¹, Uma Divakaran², Amit Dutta³, and Diptiman Sen⁴
^{1,2,3}*Department of Physics, Indian Institute of Technology Kanpur 208016, India*
⁴*Center for High Energy Physics, Indian Institute of Science, Bangalore 560012, India*

We study the quantum dynamics of a one-dimensional spin-1/2 anisotropic XY model in a transverse field when the transverse field or the anisotropic interaction is quenched at a slow but uniform rate. The two quenching schemes are called transverse and anisotropic quenching respectively. Our emphasis in this paper is on the anisotropic quenching scheme and we compare the results with those of the other scheme. In the process of anisotropic quenching, the system crosses all the quantum critical lines of the phase diagram where the relaxation time diverges. The evolution is non-adiabatic in the time interval when the parameters are close to their critical values, and is adiabatic otherwise. The density of defects produced due to non-adiabatic transitions is calculated by mapping the many-particle system to an equivalent Landau-Zener problem and is generally found to vary as $1/\sqrt{\tau}$, where τ is the characteristic time scale of quenching, a scenario that supports the Kibble-Zurek mechanism. Interestingly, in the case of anisotropic quenching, there exists an additional non-adiabatic transition, in comparison to the transverse quenching case, with the corresponding probability peaking at an incommensurate value of the wave vector. In the special case in which the system passes through a multi-critical point, the defect density is found to vary as $1/\tau^{1/6}$. The von Neumann entropy of the final state is shown to maximize at a quenching rate around which the ordering of the final state changes from antiferromagnetic to ferromagnetic.

PACS numbers: 73.43.Nq, 05.70.Jk, 75.10.Jm

I. INTRODUCTION

A quantum phase transition corresponds to a fundamental change in the symmetry of the ground state of a quantum system when the strength of the quantum fluctuations is appropriately tuned at zero temperature^{1,2}. In a quantum system, statics and dynamics are intermingled, and a quantum critical point is therefore associated with a diverging correlation length as well as a diverging relaxation time. The diverging time scale plays a non-trivial role when the system is driven through the quantum critical point at a uniform rate^{3,4,5,6,7}. This implies that no matter how slow the quenching may be, the dynamics of the system fails to be completely adiabatic when a quantum critical point is crossed. The possibility of experimental studies of non-equilibrium strongly correlated quantum systems⁸ has paved the way for rigorous theoretical investigations^{9,10,11,12,13} of the dynamics of various model Hamiltonians when swept through their quantum critical points. Recently a general analysis has been carried out of the effects of quenching in gapless systems¹⁴.

The above mentioned non-adiabaticity arising due to the diverging relaxation time near the critical point leads to the production of topological defects. The spatial distribution of the spins in the final state is quite complex in comparison to the situation in which the dynamics is adiabatic for the entire range of time. The rate of production of defects can be quantified using the prediction of the Kibble-Zurek (KZ) theory extended to quantum spin chains^{15,16}. If the gap of a one-dimensional quantum Hamiltonian is changed linearly as t/τ , where τ is the characteristic time scale of quenching, the dynamics is adiabatic for almost the entire span of time, except

for a region in the vicinity of the quantum critical point called the “impulse” region where non-adiabatic transitions dominate³. The system enters the impulse region at a time \tilde{t} when the rate of change of the gap is of the order of the relaxation time of the system. One can show that $\tilde{t} \sim \sqrt{\tau}$ which eventually results in the density of defects decreasing as $1/\sqrt{\tau}$. In other words, there is, on average, a single defect in a region of length ξ which also scales as $\sqrt{\tau}$. A smaller quenching rate (larger value of τ) yields a larger ξ and the defect production is less. A detailed analysis of the above mechanism for exactly solvable quantum spin chains is presented in Refs. 3,4,5,6,7 and 17. Recently, the above studies have been extended to explore the dynamics of disordered transverse Ising chains^{18,19}. The quenching behavior of Bose-Hubbard models has also been explored in recent years^{20,21}.

There is a recent upsurge in the study of quantum dynamics from the point of view of an optimization problem where the strength of the quantum fluctuations is quenched from a very high value to zero in order to arrive at the true ground state of a frustrated classical system. This approach of adiabatic quantum computation is popularly known as “quantum annealing”^{22,23,24}. The measure of non-adiabaticity in this approach is given by the residual energy $E_{\text{res}} = E_{\text{fin}} - E_{\text{cl}}$, where E_{fin} is the energy of the final state, and E_{cl} is the energy of the true classical ground state. The two measures of the degree of non-adiabaticity, the density of defects in the previous approach and the residual energy in the quantum annealing approach, are proportional to each other for a disorder free system. In the present literature on quantum dynamics, the terms “quenching” and “annealing” are often used synonymously.

In this work, we study the dynamics of an anisotropic

transverse XY spin-1/2 chain^{25,26,27} which is driven across various quantum critical lines at a steady and finite rate. In the transverse quenching scheme, the transverse field is varied from $-\infty$ to ∞ ^{4,6,7}, whereas in the “anisotropic quenching”, which constitutes the main theme of this paper, the interaction term is quenched from $-\infty$ to ∞ keeping the transverse field unchanged. We study the “anisotropic” quenching scheme in detail, and compare the results with those of the transverse quenching scheme. In both cases, the dynamics is exactly solved via a mapping to an equivalent Landau-Zener problem²⁸ through a Jordan-Wigner transformation from spins to fermions²⁵.

The paper is organized in the following way. In Section II, we discuss the Hamiltonian and the corresponding phase diagram. For the sake of completeness and to fix our notations and terminology at the outset, we include a brief discussion of the Jordan-Wigner transformation and the diagonalization of the spin Hamiltonian in the fermionic representation. We report the results of the transverse as well as the anisotropic quenching scheme in Section III. In Section IV, we discuss the behavior of the von Neumann entropy and the magnetization of the final state as a function of the quenching time.

II. THE MODEL AND THE PHASE DIAGRAM

The Hamiltonian of the one-dimensional anisotropic spin-1/2 XY chain in a transverse field is given by^{25,26,27}

$$H = -\frac{1}{2} \sum_n (J_x \sigma_n^x \sigma_{n+1}^x + J_y \sigma_n^y \sigma_{n+1}^y + h \sigma_n^z), \quad (1)$$

where the σ 's are Pauli spin matrices satisfying the usual commutation relations. The strength of the transverse field is denoted by h , and $J_x - J_y$ is the measure of the anisotropy of interactions in the x and y directions. In this work, J_x , J_y and h are chosen to be non-random. To explore the excitation spectrum of the Hamiltonian, we choose time-independent values of the parameters in this introductory section. In the limit $J_y = 0$, Hamiltonian in Eq. (1) reduces to the transverse Ising Model²⁹, while for $J_x = J_y$ it describes an isotropic XY model²⁵.

The Hamiltonian in Eq. (1) can be exactly diagonalized using the Jordan-Wigner transformation which maps a system of spin-1/2's to a system of spinless fermions^{25,27,30}. The Jordan-Wigner transformation of spins to fermions is given by

$$\begin{aligned} c_n &= \left(\prod_{j=-\infty}^{n-1} \sigma_j^z \right) (-1)^n \sigma_n^-, \\ c_n^\dagger &= \left(\prod_{j=-\infty}^{n-1} \sigma_j^z \right) (-1)^n \sigma_n^+, \end{aligned} \quad (2)$$

where $\sigma_n^\pm = (\sigma_n^x \pm i\sigma_n^y)/2$ are the spin raising (lowering) operators. The operator σ_n^z is expressed in terms of

fermion operators as $\sigma_n^z = 2c_n^\dagger c_n - 1$; thus the presence of a fermion at site n corresponds to a spin-up state. In the fermionic language, the above Hamiltonian can be rewritten in Fourier space with a periodic boundary condition as

$$\begin{aligned} H = & - \sum_{k>0} \{ [(J_x + J_y) \cos k + h] (c_k^\dagger c_k + c_{-k}^\dagger c_{-k}) \\ & + i(J_x - J_y) \sin k (c_k^\dagger c_{-k}^\dagger - c_{-k} c_k) \}. \end{aligned} \quad (3)$$

This Hamiltonian is quadratic in the c operators and can therefore be diagonalized using the standard Bogoliubov transformation; we then arrive at an expression for the gap in the excitation spectrum given by^{25,27}

$$\epsilon_k = [h^2 + J_x^2 + J_y^2 + 2h(J_x + J_y) \cos k + 2J_x J_y \cos 2k]^{1/2}. \quad (4)$$

The gap given in Eq. (4) vanishes at $h = \mp(J_x + J_y)$ for wave vectors $k = 0$ and π respectively; it turns out that this signals a quantum phase transition from a quantum paramagnetic phase to a ferromagnetically ordered phase in which a discrete Z_2 symmetry of the Hamiltonian in Eq. (1) ($\sigma_n^x \rightarrow -\sigma_n^x$, $\sigma_n^y \rightarrow -\sigma_n^y$ and $\sigma_n^z \rightarrow \sigma_n^z$ for all n) is spontaneously broken. This transition belongs to the universality class of the transverse Ising model^{27,29} and is therefore referred to as the “Ising” transition. The spectrum is also gapless in the limit when the anisotropy vanishes, $J_x \rightarrow J_y$, provided that $|h/2J_x| \leq 1$. The line $J_x = J_y$ marks the phase boundary between two ferromagnetically ordered phases denoted by FM_x and FM_y , and the corresponding phase transition is called the “anisotropic transition”. In the FM_x phase, $J_x > J_y$ and hence the ferromagnetic ordering is in the x direction, while it is the other way around in the FM_y phase. One can also check that the long-range order in the FM_x or FM_y phase only exists for a relatively weak transverse field lying in the range $-J_x - J_y < h < J_x + J_y$. Each ferromagnetically ordered phase is further divided into a commensurate and an incommensurate region with the incommensurate wave vector k_0 given by

$$\cos k_0 = -\frac{h(J_x + J_y)}{4J_x J_y}. \quad (5)$$

On the anisotropic phase boundary $J_x = J_y$, the incommensurate wave vector therefore has a value $k_0 = \cos^{-1}(-h/2J_x)$. The boundary between these two regions inside a ferromagnetic phase is given by the relation $h/(J_x + J_y) = \pm(1 - \gamma^2)$, with $\gamma \equiv (J_x - J_y)/(J_x + J_y)$, as shown by the thick dashed lines in Fig. 1. The exponents associated with the anisotropic transition are different from the Ising case and are identical to the exponents of a pair of decoupled Ising models^{26,27}.

We note that the points corresponding to $J_x = J_y$ and $h = \pm 2J_y$ are multi-critical points since more than one phase boundary passes through them. We will see later that the quenching dynamics shows a different behavior when the system passes through those points.

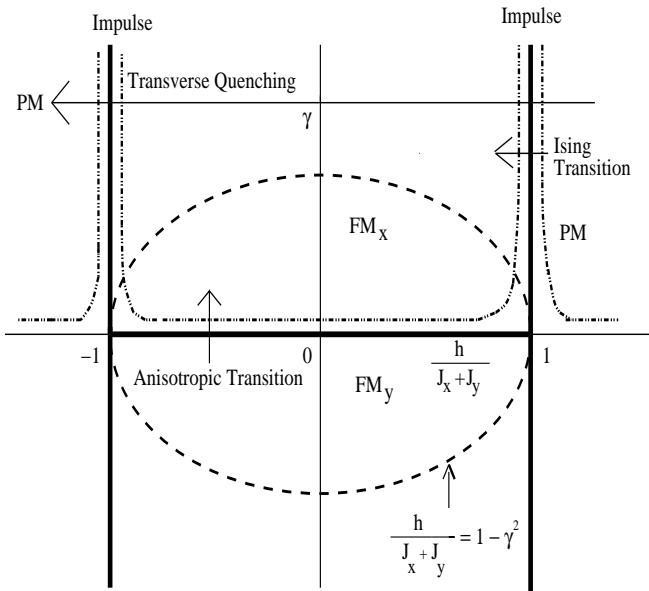


FIG. 1: The phase diagram of the anisotropic XY model in a transverse field in the $h/(J_x + J_y) - \gamma$ plane. The vertical bold lines given by $h/(J_x + J_y) = \pm 1$ denote the Ising transitions. The system is also gapless on the horizontal bold line $J_x = J_y$ for $|h| < J_x + J_y$. FM_x (FM_y) is a long-range ordered phase with ferromagnetic ordering in the x (y) direction. The thick dashed line marks the boundary between the commensurate and incommensurate ferromagnetic phase. The thin dotted lines indicate the adiabatic and impulse regions when the field h is quenched from $-\infty$ to ∞ .

III. QUENCHING SCHEME AND RESULTS

In this section, we will discuss the results obtained for the quenching dynamics of the Hamiltonian in Eq. (1) for two different schemes. In the first scheme, the time-dependent transverse field is of the form $h(t) = t/\tau$, where t is varied from $-\infty$ to ∞ , and τ is the characteristic time scale of quenching, often referred to as the “quenching time”. This “transverse quenching” scheme has been studied extensively for the XY chain by Cherng and Levitov⁶, and for the transverse Ising case by Dziarmaga⁴ and by Polkovnikov⁷. We shall briefly present the results for the transverse quenching which will be helpful in comparing it with the results obtained in the other scheme, namely, the “anisotropic quenching”.

As mentioned in the Introduction, in the “anisotropic quenching” scheme, the interaction term $J_x (= t/\tau)$ is quenched from a very large negative initial value to a very large positive final value, with J_y and h held fixed at some positive values. For our numerical studies, we will set $2J_y > h$ for the reason explained below. In the initial state, all the spins are antiferromagnetically ordered in the x direction. On the other hand, the final state should correspond to a state with a perfect ferromagnetic order in the x direction had the dynamical evolution been adi-

abatic for the entire span of time. However, due to the non-adiabatic transitions near the quantum critical regions, the final state in the limit $t \rightarrow \infty$ will not be perfectly ordered and will include a finite fraction of kinks or spins aligned anti-parallel to the direction of ordering.

The Hamiltonian in Eq. (3) decouples into a sum of independent terms, $H(t) = \sum_{k>0} H_k(t)$, where each $H_k(t)$ operates on a four-dimensional Hilbert space spanned by the basis vectors $|0\rangle$, $|k\rangle = c_k^\dagger|0\rangle$, $|-k\rangle = c_{-k}^\dagger|0\rangle$, and $|k, -k\rangle = c_k^\dagger c_{-k}^\dagger|0\rangle$. The vacuum state where no c -particle is present is denoted by $|0\rangle$ which corresponds to a spin configuration with all spins pointing in the $-z$ direction. The occurrence of only bilinear terms like $c_k^\dagger c_{-k}^\dagger$ in the Hamiltonian in (3) ensures that the parity (even or odd) of the total number of fermions given by $n_k = c_k^\dagger c_k + c_{-k}^\dagger c_{-k}$ is conserved for each value of $k > 0$. Thus the states $|0\rangle$ and $|k, -k\rangle$ are coupled to each other by the Hamiltonian, while the states $|k\rangle$ and $|-k\rangle$ remain invariant.

To study the dynamics of transverse quenching, it is sufficient to project the Hamiltonian $H_k(t)$ to the two-dimensional subspace spanned by $|0\rangle$ and $|k, -k\rangle$ since the ground state of Eq. (3) for each value of k lies within this subspace. In this subspace, the Hamiltonian takes the form

$$H_k(t) = -[h + (J_x + J_y) \cos k] I_2 + \begin{bmatrix} h + (J_x + J_y) \cos k & i(J_x - J_y) \sin k \\ -i(J_x - J_y) \sin k & -h - (J_x + J_y) \cos k \end{bmatrix},$$

where I_2 denotes the 2×2 identity matrix. A state in this subspace can be represented as a linear superposition $\psi_k(t) = u_k(t)|0\rangle + v_k(t)|k, -k\rangle$, where the amplitudes $u_k(t)$ and $v_k(t)$ are time-dependent. The initial condition in the transverse quenching scheme is given by $u_k(-\infty) = 1$ and $v_k(-\infty) = 0$. The time evolution of a generic state is governed by the Schrödinger equation

$$i\partial_t \psi_k(t) = H_k(t) \psi_k(t). \quad (6)$$

The projection of the Hamiltonian to the 2×2 Hilbert space has effectively reduced the many-body problem to the problem of a two-level system. The off-diagonal term of the projected Hamiltonian, $\Delta = i(J_x - J_y) \sin k$, represents the interaction between the two time-dependent levels $E_{1,2} = \pm[h(t) + (J_x + J_y) \cos k]$. The Schrödinger equation given above is identical to the Landau-Zener problem of a two-level system, where the off-diagonal terms of the Hamiltonian determines the non-adiabatic transition probability p_k for the wave vector k . Using the Landau-Zener transition formula, this transition probability of excitations at the final time is given by²⁴

$$p_k = e^{-2\pi\tilde{\gamma}}, \quad (7)$$

where $\tilde{\gamma} = \Delta^2 / |\frac{d}{dt}(E_1 - E_2)|$. Equivalently, p_k determines the probability that the system remains in the initial state $|0\rangle$ at the final time. For the transverse quench-

ing case, one can use the relation in Eq. (7) to obtain p_k as a function of the anisotropy term $J_x - J_y$ and τ as⁶

$$p_k = e^{-\pi\tau(J_x - J_y)^2 \sin^2 k}. \quad (8)$$

This leads to an expression for the density of kinks n generated due to non-adiabatic transitions,

$$n = \int_0^\pi \frac{dk}{\pi} p_k \simeq \frac{1}{\pi\sqrt{\tau} |J_x - J_y|}. \quad (9)$$

Eq. (9) shows that the kink density decreases as $1/\sqrt{\tau}$ for large τ as predicted by the Kibble-Zurek theory and proved by Cherg and Levitov in the case of transverse quenching⁶.

We shall now focus on the anisotropic quenching scheme where the interaction term $J_x(t) = t/\tau$ is changed from $-\infty$ to ∞ , with J_y and h held fixed at some positive values. Let us first point out the range in time where the system fails to follow the instantaneous ground state (namely, the region where the relaxation time is large or divergent) as J_x is varied. If $J_x(t_1) + J_y = -h$, i.e., for $t_1 = -\tau(h + J_y)$, the system undergoes an Ising transition from the initial antiferromagnetic phase to a paramagnetic phase. When J_x is further increased so that $J_x(t_2) + J_y = h$, i.e., for $t_2 = (h - J_y)\tau$, there is a phase transition from the paramagnetic to FM_y phase. It is to be noted however, that for $J_x = -J_y$, there is no further anisotropic transition since the magnitude of h is greater than $J_x + J_y = 0$, and the system stays paramagnetic. Eventually, at a time t_3 given by $J_x(t_3) = J_y$, with $h < 2J_y$, the system evolves to the FM_x phase. The non-adiabaticity dominates in the vicinity of these three quantum critical points, i.e., for t close to t_1, t_2 and t_3 . One should also note that if we fix $h > 2J_y$ at the outset, there cannot be any anisotropic transition, and the system directly evolves from the paramagnetic phase to the FM_x phase through the Ising transition only; hence there are two, rather than three, regions of non-adiabaticity. All the transition points are depicted in the static phase diagram of the model shown in Fig. 1. The adiabatic and non-adiabatic regions of time evolution are shown schematically in Fig. 2.

As mentioned already, in the anisotropic case, the reduced Hamiltonian in the $|0\rangle, |k, -k\rangle$ subspace includes a time-dependent J_x term with static positive values of J_y and h . The eigenstates of the Hamiltonian in the limit $t \rightarrow \pm\infty$ are

$$|e_{1k}\rangle = \sin(k/2)|0\rangle + i \cos(k/2)|k, -k\rangle$$

and

$$|e_{2k}\rangle = \cos(k/2)|0\rangle - i \sin(k/2)|k, -k\rangle,$$

with eigenvalues $\lambda_1 = t/\tau$ and $\lambda_2 = -t/\tau$ respectively; the system is in the state $|e_{1k}\rangle$ initially. A general state vector can be expressed as a linear combination of $|e_{1k}\rangle$ and $|e_{2k}\rangle$,

$$|\psi_k(t)\rangle = C_{1k}(t)|e_{1k}\rangle + C_{2k}(t)|e_{2k}\rangle. \quad (10)$$

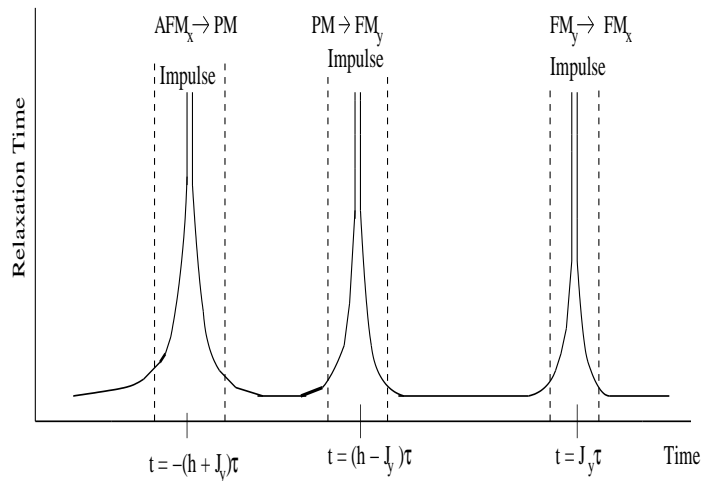


FIG. 2: Schematic diagram showing the divergence of the relaxation time of the quantum Hamiltonian at the quantum critical points. As discussed in the text, the dotted vertical lines denote the impulse region of dynamics where non-adiabatic transitions play a prominent role.

The initial condition in the anisotropic case is $C_{1k}(-\infty) = 1$ and $C_{2k}(-\infty) = 0$. The amplitudes u_k and v_k are related to the new coefficients as

$$\begin{aligned} u_k &= C_{1k} \sin(k/2) + C_{2k} \cos(k/2), \\ v_k &= iC_{1k} \cos(k/2) - iC_{2k} \sin(k/2). \end{aligned} \quad (11)$$

The Landau-Zener transition probability can be obtained by numerically solving the Schrödinger equation in Eq. (6) using the basis vectors $|0\rangle$ and $|k, -k\rangle$, with the appropriate initial conditions for u_k and v_k . The non-adiabatic transition probability p_k at the final time is simply given by $p_k = |C_{1k}(\infty)|^2$. We have shown the variation of p_k with k obtained through numerical integration in Fig. 3.

The situation is apparently complicated in the anisotropic quenching case because the off-diagonal terms of the 2×2 Hamiltonian matrix in the $|0\rangle$ and $|k, -k\rangle$ basis are time-dependent. However, by an unitary transformation to the new set of basis vectors $|e_{1k}\rangle$ and $|e_{2k}\rangle$, one can get rid of the time-dependence of the off-diagonal terms and map the anisotropic quenching problem to an equivalent Landau-Zener problem. The unitary transformation is given by $H'_k(t) = U^\dagger H_k(t)U$, where

$$U = \begin{bmatrix} \cos(k/2) & \sin(k/2) \\ -i \sin(k/2) & i \cos(k/2) \end{bmatrix},$$

and the new Hamiltonian is

$$\begin{aligned} H'_k(t) &= - [h + (J_x + J_y) \cos k] I_2 \\ &+ \begin{bmatrix} J_x + J_y \cos 2k + h \cos k & J_y \sin 2k + h \sin k \\ J_y \sin 2k + h \sin k & -J_x - J_y \cos 2k - h \cos k \end{bmatrix}. \end{aligned}$$

Therefore, the anisotropic quenching is now placed on the same footing as the transverse quenching case, with

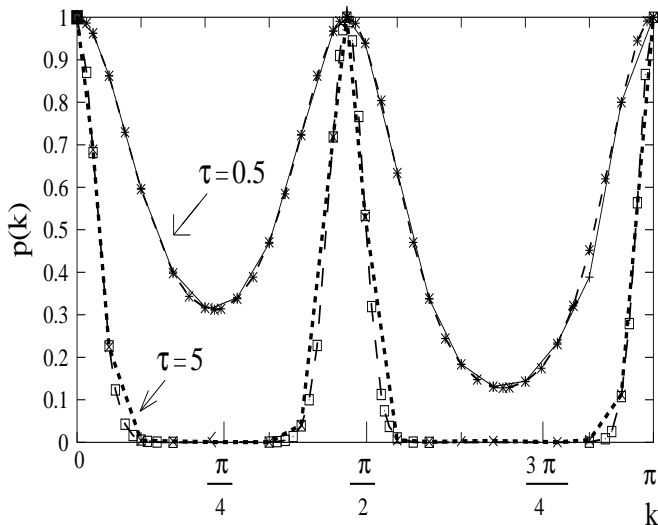


FIG. 3: p_k vs k as obtained numerically and analytically for τ equal to 0.5 and 5. We have fixed $J_y = 1$ and $h = 0.2$. In the region marked $\tau = 0.5$, the solid line is numerical and dashed line is analytical. In the region marked $\tau = 5$, the dashed line with smaller spacing is numerical and dashed line with larger spacing is analytical.

off-diagonal terms in the Hamiltonian matrix which are time-independent. The time evolution of the amplitudes $C_{1k}(t)$ and $C_{2k}(t)$ is dictated by the Schrödinger equation,

$$\begin{aligned}
 i \frac{dC_{1k}}{dt} &= (J_x(t) + J_y \cos 2k + h \cos k) C_{1k}(t) \\
 &\quad + (J_y \sin 2k + h \sin k) C_{2k}(t) \\
 i \frac{dC_{2k}}{dt} &= (J_y \sin 2k + h \sin k) C_{1k}(t) \\
 &\quad - (J_x(t) + J_y \cos 2k + h \cos k) C_{2k}(t), \quad (12)
 \end{aligned}$$

where we have dropped the effect of the term involving the identity matrix in the Hamiltonian since this affects C_{1k} and C_{2k} by the same time-dependent phase factor, and will therefore have no effect on the density matrix. The non-adiabatic transition probability now depends on J_y and h , and is given by

$$p_k = |C_{1k}(\infty)|^2 = e^{-\pi\tau(J_y \sin 2k + h \sin k)^2}. \quad (13)$$

In Fig. 3, we plot p_k as a function of the wave vector k along with the numerical results. We see that in contrast to the transverse case, there is an additional region of non-adiabaticity peaked at the incommensurate wave vector $k_0 = \cos^{-1}(-h/2J_y)$. This non-adiabaticity arises due to the existence of the anisotropic transition of the underlying static XY model at $J_x(t) = J_y$. The situation with zero transverse field is a special case where the regions of non-adiabaticity peak at $k = 0, \pi/2$ and π , respectively.

As in the transverse quenching case, we now measure

the density of kinks given by

$$n = \int_0^\pi \frac{dk}{\pi} p_k = \int_0^\pi \frac{dk}{\pi} e^{-\pi\tau(J_y \sin 2k + h \sin k)^2}. \quad (14)$$

In Fig. 4, the plot of the kink density as a function of the quenching time τ is shown, which clearly shows that $n \propto 1/\sqrt{\tau}$ for large values of τ . This finding supports the prediction of the Kibble-Zurek mechanism even in the anisotropic quenching case. One can also find an approximate analytical form of n in the following way: for large τ , only the modes very close to the critical modes contribute. For $k \rightarrow 0$ and π , p_k can be approximated as $\exp[-\pi\tau(2J_y + h)^2 k^2]$ and $\exp[-\pi\tau(2J_y - h)^2(\pi - k)^2]$ respectively. With this p_k , the density of kinks produced by the modes near $k = 0$ and π is given by

$$n_1 \simeq \frac{1}{2\pi\sqrt{\tau}} \left[\frac{1}{2J_y + h} + \frac{1}{2J_y - h} \right] = \frac{2J_y}{\pi\sqrt{\tau}(4J_y^2 - h^2)}.$$

By expanding around k_0 , we find that the contribution to n from modes with $k \sim k_0$ is equal to the contribution from $k = 0$ and $k = \pi$ taken together,

$$\begin{aligned}
 n_2 &\simeq \int_0^\pi \frac{dk}{\pi} e^{-\pi\tau(2J_y \cos 2k_0 + h \cos k_0)^2 (k - k_0)^2} \\
 &\simeq \frac{1}{\pi\sqrt{\tau}} \frac{1}{|2J_y \cos 2k_0 + h \cos k_0|}.
 \end{aligned}$$

Therefore the total kink density is given by

$$n = n_1 + n_2 \simeq \frac{4J_y}{\pi\sqrt{\tau}(4J_y^2 - h^2)}. \quad (15)$$

Fig. 4 shows that this approximate form embraces the exact result perfectly in the limit of large τ .

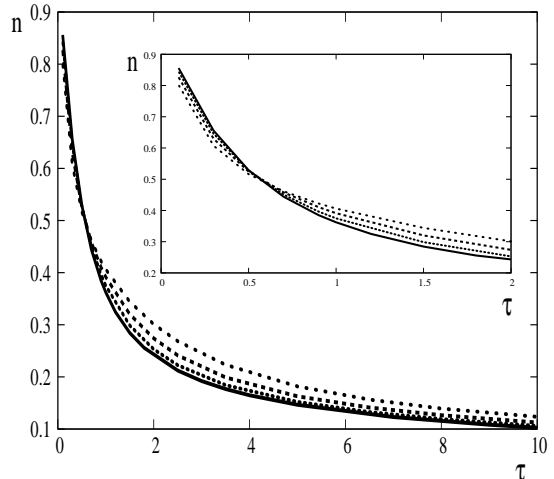


FIG. 4: Variation of kink density n with τ as obtained by numerical integration of Eq. (14) for $h = 0.2, 0.4, 0.6, 0.8$ (from bottom to top in the large τ region), with $J_y = 1$. For large τ , n increases with increasing h , whereas for small τ , it decreases with increasing h as shown in the inset.

Using Eq. (15), one can find the variation of the kink density with h , for large values of τ , as

$$\frac{\partial n}{\partial h} \simeq \frac{8hJ_y}{\pi\sqrt{\tau}(4J_y^2 - h^2)^2}.$$

The slope is positive for all values h indicating an increment in kink density with increasing h as shown in Fig. 4. On the other hand, for small τ , the density n is found to decrease with increasing h . In the limit $\pi\tau(J_y \sin 2k + h \sin k)^2 \ll 1$, one can expand the exponential in p_k in Eq. (14), retaining only terms up to first order in τ . One can then show that $\partial n/\partial h$ is negative. The crossover from the small τ to the large τ behavior occurs around a typical quenching time $\tau = \ln 2/[\pi(J_y \sin 2k + h \sin k)^2]$. The significance of the crossover time is explained below.

To derive a characteristic time scale of the anisotropic quenching, we first note that the minima of the probability p_k occurs at a wave vector value \tilde{k} , where

$$\cos \tilde{k} = \frac{-h \pm \sqrt{h^2 + 32J_y^2}}{8J_y}. \quad (16)$$

The presence of a non-zero transverse field h leads to an asymmetry in p_k on the either side of the maxima at k_0 as is evident at smaller values of τ (Fig. 3). We now define a time scale τ_0 so that at $\tau = \tau_0$, $p_k = 1/2$ at the minima⁶ $k = \tilde{k}$. This implies

$$\tau_0 = \frac{\ln 2}{\pi(J_y \sin 2\tilde{k} + h \sin \tilde{k})^2}. \quad (17)$$

The two conjugate values of \tilde{k} given in Eq. (16) lead to a pair of τ_0 's for the anisotropic quenching, in contrast to the transverse quenching case. For $h = 0$, these two values coalesce into one. The crossover of density shown in Fig. 4, takes place roughly around the smaller value of τ_0 denoted by τ_{02} . For $\tau \gg \tau_{01}, \tau_{02}$, the dynamics is nearly adiabatic except for the modes very close to the critical modes (Fig. 5).

Eq. (15) is valid for $2J_y > h$. On the other hand, if we take $h > 2J_y$, the system evolves directly from the paramagnetic to the FM_x phase; there is no anisotropic transition. In this case, Eq. (14) gives the kink density to be

$$n \simeq \frac{1}{2\pi\sqrt{\tau}} \left[\frac{1}{h + 2J_y} + \frac{1}{h - 2J_y} \right] = \frac{h}{\pi\sqrt{\tau}(h^2 - 4J_y^2)}.$$

(Note that $\partial n/\partial h$ is negative in this case). The transverse Ising model result given in Ref. 4 can be obtained by setting $J_y = 0$ in the above expression.

Finally, we consider what happens if $1 - 2J_y/h$ is close to zero. If $2J_y = h$, the system passes through a multicritical point when $J_x(t)$ equals J_y ; we therefore expect an unusual behavior of the kink density n in this case. If $2J_y = h$ and τ is large, we find that Eq. (14) is dominated by the region near $k = \pi$; since p_k can be approximated there by $\exp[-\pi\tau h^2(\pi - k)^6/4]$, the contribution of this

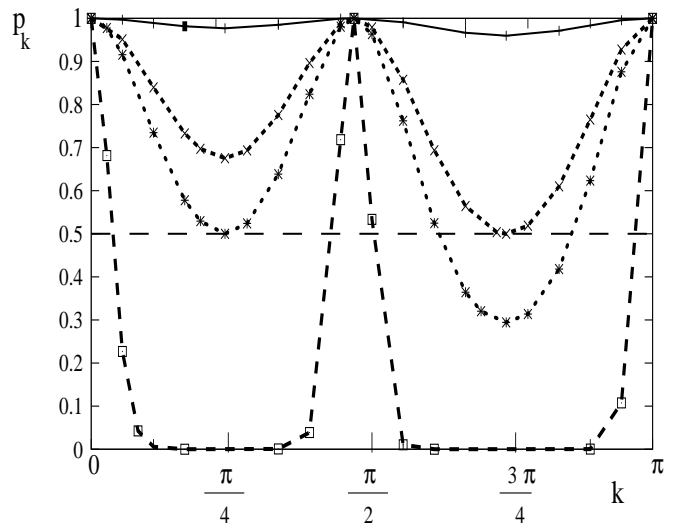


FIG. 5: Variation of p_k vs k for $\tau = 5, \tau_{01}, \tau_{02}$ and 0.01 from bottom to top, where $p_k = 0.5$ at the two minima for $\tau = \tau_{01}$ and τ_{02} . We have fixed $J_y = 1$ and $h = 0.2$. For $\tau \gg \tau_{01}, \tau_{02}$, the evolution is almost adiabatic except at $k = 0, \pi$ and k_0 , where the system remains frozen in its initial state. For very small τ , p_k is close to 1 for all k .

region to n goes as $1/(h^{1/3}\tau^{1/6})$. [The contribution from the region near $k = 0$ to n goes as $1/(h\sqrt{\tau})$ which is much smaller than $1/(h^{1/3}\tau^{1/6})$ if $h^2\tau \gg 1$.] Now, if $1 - 2J_y/h$ is non-zero but small, p_k can be approximated near $k = \pi$ by $\exp[-\pi\tau\{(h - 2J_y)(\pi - k) + h(\pi - k)^3/2\}^2]$. We then see that the term $\tau(h - 2J_y)^2(\pi - k)^2$ will become more important than the term $\tau h^2(\pi - k)^6$ and the kink density will show a crossover from a $1/\tau^{1/6}$ behavior to a $1/\sqrt{\tau}$ behavior when τ increases beyond a value which is of order $h/|h - 2J_y|^3$.

IV. ENTROPY AND MAGNETIZATION OF THE FINAL STATE

The quenching dynamics of the spin model is dictated by the Schrödinger equation and is obviously unitary. Therefore, the final state must be a pure state described by a density matrix of the product form $\rho = \bigotimes \rho_k$, where ρ_k is given by

$$\begin{bmatrix} p_k & q_k \\ q_k^* & 1 - p_k \end{bmatrix}, \quad (18)$$

and $q_k = C_{1k}(\infty)C_{2k}^*(\infty)$. The diagonal elements of the reduced 2×2 density matrix are smooth functions of k and are independent of the total time of quenching (which we now set equal to T for convenience, with $T \gg 1$), whereas the off-diagonal terms are rapidly oscillating functions of both k and T .

The final state, even though a pure state, has a fairly complicated local structure; its local properties in the real space is identical to that of a mixed state with a finite entropy⁶. In other words, the final state can be

viewed as a superposition of different configurations of magnetically ordered domains. The off-diagonal terms of the density matrix ρ_k can be made to vanish at the final time T upon coarse-graining in the wave vector k . The final state therefore may be viewed locally as a mixed state described by a decohered reduced density matrix ρ_D given by

$$\begin{bmatrix} p_k & 0 \\ 0 & 1 - p_k \end{bmatrix}. \quad (19)$$

To quantify the amount of information lost in the decoherence process, we consider the von Neumann entropy density of the system, $s = -\text{tr}(\rho_D \ln \rho_D)$, namely,

$$s = - \int_0^\pi \frac{dk}{\pi} [p_k \ln(p_k) + (1 - p_k) \ln(1 - p_k)]. \quad (20)$$

In the case of the transverse quenching⁶, the maximum of the entropy density occurs near the value of $\tau = 2\tau_0$ where the minimum value of $p_k = 1/2$. In the anisotropic case, as mentioned already, τ_0 is non-unique (Fig. 5). The entropy density s when plotted against τ/τ_{02} shows a maxima at a quenching rate $\tau \sim 2\tau_{02}$ (see Fig. 6), while no special behavior is noted near τ_{01} ; this establishes τ_{02} as the characteristic time scale of the anisotropic quenching. For sufficiently small τ , non-adiabaticity dominates and the system stays in its initial state with high probability, namely, the system more or less retains its initial antiferromagnetic ordering even at the final time. The system looks like a pure state even at small length scales. In the large τ limit, on the other hand, the system evolves essentially in an adiabatic way to the final ground state, and the non-adiabatic transition probability is small. The final state is ferromagnetically ordered. Therefore, the entropy density vanishes asymptotically for both large and small values of τ , and the maximum occurs at an intermediate value of $\tau \sim 2\tau_{02}$ where the defect in the local ordering of the final state is maximum.

The above arguments can be justified further by exploring the magnetization of the system in the final state. Let us recall that the initial state is antiferromagnetically oriented in the x direction. The average energy of the mode k at the final time is related to p_k as $(2p_k - 1)J_x$; hence, integrating over all the modes gives the total energy per site to be $(2n - 1)J_x$, where n is the density of kinks defined above. On the other hand, at the final time, $J_x \gg J_y$ and h ; hence the effective Hamiltonian is $H = -\sum_n J_x \sigma_n^x \sigma_{n+1}^x$, and the total energy density is $-J_x m_x^2$. Putting all this together and using Eq. (15), we arrive at an expression for the magnetization,

$$m_x(t \rightarrow \infty) \simeq \left(1 - \frac{8J_y}{\pi\sqrt{\tau} (4J_y^2 - h^2)} \right)^{1/2}, \quad (21)$$

and $m_x = 0$ whenever the right hand side of Eq. (21) is imaginary. In Fig. 6, we plot the final magnetization as a function of τ/τ_{02} which shows that the magnetization starts to become non-zero when the quenching time is of

the order of $2\tau_{02}$. For slower quenching (larger values of τ), the dynamics tends to be more and more adiabatic, and the final magnetization monotonically increases towards the saturation value of unity.

Let us now shift our attention to the behavior of the staggered magnetization m_{sx} . In the limit of small τ , the system fails to follow the instantaneous Hamiltonian; hence the final state retains an antiferromagnetic order with vanishing total magnetization. In other words, the total magnetization of the even sites cancels the total magnetization of the odd sites. Using similar arguments as given above, the staggered magnetization can be shown to behave as $(2n - 1)^{1/2}$; hence it vanishes at $n = 1/2$ and stays at zero for smaller values of n (i.e., higher values of τ). On the other hand, for smaller values of τ , $n > 1/2$ and there is a non-zero value of m_{sx} . Fig. 6 shows that the staggered magnetization of the final state vanishes at a quenching rate close to $2\tau_0$ where the ferromagnetic order starts to set in.

We can use similar arguments as given in the case of entropy density to understand the variation of the magnetization with τ as presented above. We have argued already that even though the final state is a pure state, it can also be viewed locally, or with a coarse-grained wave vector scale, as a decohered (mixed) state. If the quenching time scale $\tau \ll \tau_{02}$, there are very few local defects and the system retains the initial antiferromagnetic order. On the other hand, for $\tau \gg \tau_{02}$, the final state is locally ferromagnetically ordered. Hence, there exists an intermediate region of $\tau \sim \tau_{02}$ where the antiferromagnetic order decreases rapidly. Eventually, for $\tau \gtrsim 2\tau_{02}$, the final state starts to acquire ferromagnetic ordering.

V. CONCLUSIONS

We have studied the adiabatic quantum dynamics of an anisotropic XY spin-1/2 chain in a transverse field when the parameters of the Hamiltonian are quenched at a steady and finite rate. Our emphasis lies on a new scheme, namely, the anisotropic quenching, where the interaction strength in the x direction is quenched from $-\infty$ to ∞ at a uniform rate dictated by a time scale τ . At first sight, the Landau-Zener theory does not seem to be applicable in this case due to the presence of time-dependent off-diagonal terms in the reduced 2×2 Hamiltonian. However, through a unitary transformation to an appropriate basis, the time dependence can be entirely shifted to the diagonal terms, and Landau-Zener theory turns out to be applicable once again.

In the process of the anisotropic quenching, the system is swept across all the three quantum critical lines in the phase diagram if $h < 2J_y$, and across two quantum critical lines if $h > 2J_y$. In both these cases, the density of defects is found to vary as $1/\sqrt{\tau}$. In the special case of $h = 2J_y$, the system is swept across a multi-critical point, and the density of defects is found to vary as $1/\tau^{1/6}$.

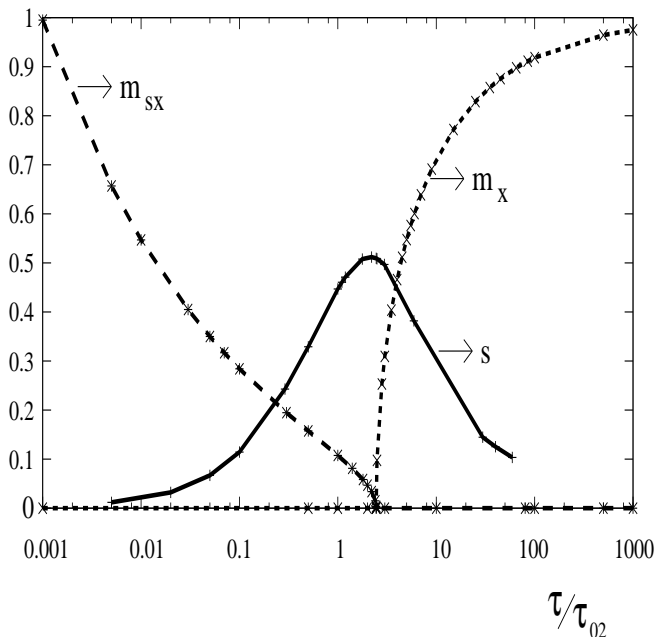


FIG. 6: Variation of von Neumann entropy density s , staggered magnetization m_{sx} and magnetization m_x as a function of τ/τ_{02} , for $J_y = 1$ and $h = 0.2$.

Finally, we find a characteristic quenching time τ_{02} around which the von Neumann entropy of the final state maximizes and ferromagnetic ordering starts to set in. The residual energy of the final state is proportional to the defect density and hence scales as $1/\sqrt{\tau}$.

Acknowledgments

A.D. acknowledges J. K. Bhattacharjee, B. K. Chakrabarti, A. Das and K. Sengupta for interesting discussions. D.S. thanks DST, India for financial support under the project SP/S2/CMP-27/2006.

E-mail: ¹victor@iitk.ac.in
²udiva@iitk.ac.in
³dutta@iitk.ac.in,
⁴diptiman@cts.iisc.ernet.in

-
- ¹ S. Sachdev, *Quantum Phase Transitions* (Cambridge University Press, Cambridge, 1999).
- ² B. K. Chakrabarti, A. Dutta, and P. Sen, *Quantum Ising Phases and Transitions in Transverse Ising Models*, **m41** (Springer-Verlag, Berlin, 1996).
- ³ W. H. Zurek, U. Dorner, and P. Zoller, Phys. Rev. Lett. **95**, 105701 (2005).
- ⁴ J. Dziarmaga, Phys. Rev. Lett. **95**, 245701 (2005).
- ⁵ B. Damski, Phys. Rev. Lett. **95**, 035701 (2005).
- ⁶ R. W. Cherng and L. S. Levitov, Phys. Rev. A **73**, 043614 (2006).
- ⁷ A. Polkovnikov, Phys. Rev. B **72**, 161201(R) (2005).
- ⁸ M. Greiner, O. Mandel, T. Esslinger, T. W. Hänsch, and I. Bloch, Nature (London) **415**, 39 (2002); T. Stöferle, H. Moritz, C. Schori, M. Köhl, and T. Esslinger, Phys. Rev. Lett. **92**, 130403 (2004); V. M. H. Ruutu, V. B. Eltsov, A. J. Gill, T. W. B. Kibble, M. Krusius, Yu. G. Makhlin, B. Placais, G. E. Volovik, and Wen Xu, Nature (London) **382**, 334 (1996); C. Bäuerle, Yu. M. Bunkov, S. N. Fisher, H. Godfrin, and G. R. Pickett, Nature (London) **382**, 332 (1996); R. Carmi, E. Polturak, and G. Koren, Phys. Rev. Lett. **84**, 4966 (2000).
- ⁹ K. Sengupta, S. Powell, and S. Sachdev, Phys. Rev. A **69**, 053616 (2004).
- ¹⁰ P. Calabrese and J. Cardy, J. Stat. Mech: Theory Expt P04010 (2005).
- ¹¹ A. Das, K. Sengupta, D. Sen, and B. K. Chakrabarti, Phys. Rev. B **74**, 144423 (2006).
- ¹² L. Cincio, J. Dziarmaga, M. M. Rams, and W. H. Zurek, Phys. Rev. A, **75**, 052321 (2007).
- ¹³ M. Cramer, C. M. Dawson, J. Eisert, and T. J. Osborne, arXiv:cond-mat/0703314.
- ¹⁴ A. Polkovnikov and V. Gritsev, arXiv:0706.0212.
- ¹⁵ T. W. B. Kibble, J. Phys. A **9**, 1387 (1976).
- ¹⁶ W. H. Zurek, Nature (London) **317**, 505 (1985); Phys. Rep. **276**, 177 (1996).
- ¹⁷ B. Damski and W. H. Zurek, Phys. Rev. A **73**, 063405 (2006).
- ¹⁸ J. Dziarmaga, Phys. Rev. B **74**, 064416 (2006).
- ¹⁹ T. Caneva, R. Fazio, and G. E. Santoro, arXiv:0706.1832.
- ²⁰ F. M. Cucchietti, B. Damski, J. Dziarmaga, and W. H. Zurek, Phys. Rev. A **75**, 023603 (2007).
- ²¹ R. Schützhold, M. Uhlmann, Y. Xu, and U. R. Fischer, Phys. Rev. Lett. **97**, 200601 (2006).
- ²² T. Kadowaki and H. Nishimori, Phys. Rev. E **58**, 5355 (1998).
- ²³ *Quantum Annealing and Related Optimization Methods*, Ed. by A. Das and B. K. Chakrabarti (Springer-Verlag, Berlin, 2005).
- ²⁴ S. Suzuki and M. Okada, in *Quantum Annealing and Related Optimization Methods*, Ed. by A. Das and B. K. Chakrabarti (Springer-Verlag, Berlin, 2005).
- ²⁵ E. Lieb, T. Schultz, and D. Mattis, Ann. Phys. (NY) **16**, 407 (1961).
- ²⁶ E. Barouch and B. M. McCoy, Phys. Rev. A **3**, 786 (1971).
- ²⁷ J. E. Bunder and R. H. McKenzie, Phys. Rev. B **60**, 344 (1999).
- ²⁸ C. Zener, Proc. Roy. Soc. London Ser A **137**, 696 (1932); L. D. Landau and E. M. Lifshitz, *Quantum Mechanics: Non-relativistic Theory*, 2nd ed. (Pergamon Press, Oxford, 1965).
- ²⁹ P. Pfeuty, Ann. Phys. (NY) **57**, 79 (1970).
- ³⁰ J. B. Kogut, Rev. Mod. Phys. **51**, 659 (1979).